Atmos. Meas. Tech. Discuss., 2, 1625–1662, 2009
www.atmos-meas-tech-discuss.net/2/1625/2009/

Atmospheric Measurement Techniques Discussions is the access reviewed discussion forum of *Atmospheric Measurement Techniques*

Quality assessment of Izaña's upper-air water vapour measurement techniques: FTIR, Cimel, MFRSR, GPS, and Vaisala RS92

M. Schneider[1], **P. M. Romero**[2], **F. Hase**[1], **T. Blumenstock**[1], **E. Cuevas**[2], **and R. Ramos**[2]

[1]IMK-ASF, Forschungszentrum und Universität Karlsruhe, Karlsruhe, Germany
[2]Centro de Investigación Atmosférica de Izaña, Agencia Estatal de Meteorología, Spain

Received: 11 May 2009 – Accepted: 2 July 2009 – Published: 13 July 2009

Correspondence to: M. Schneider (matthias.schneider@imk.fzk.de)

Published by Copernicus Publications on behalf of the European Geosciences Union.

Abstract

At the Izaña Atmospheric Research Centre water vapour amounts are measured routinely by different techniques since many years. We intercompare the total precipitable water vapour amounts measured between 2005 and 2009 by a Fourier Transform Infrared (FTIR) spectrometer, a Multifilter rotating shadow-band radiometer (MFRSR), a Cimel sunphotometer, a Global Positioning System (GPS) receiver, and daily radiosondes (Vaisala RS92). In addition we intercompare the water vapor profiles measured by the FTIR and the radiosondes. The long-term intercomparison assures that our study well represents the large water vapour variabilities that occur in the troposphere and allows a reliable empirical quality assessment for the different water vapour dataset. We examine how the data quality of the different techniques depends on atmospheric conditions and estimate the dry bias of the techniques which are restricted to clear sky observations.

1 Introduction

In the troposphere water vapour is the most important trace gas. It is a key player in governing tropospheric dynamics, i.e. weather, and is a prime greenhouse gas. Observing and analysing its evolution is needed for a better understanding of past and future climate. The water vapour feedback effect (a rising atmospheric temperature increases the water vapour amounts, which on its part causes a further temperature rise) plays a central role in climate modeling. It amplifies the temperature rise caused by CO_2 by a factor of approx. 1.7 (Held and Soden, 2000). The evolution of the water vapour content in the tropics and the subtropics is of particular importance, since the Earth's climate is in particular sensible to water vapour changes in the dry regions of the tropics and the subtropics (Pierrehumbert, 1995, 2000).

In contradiction to the importance of the tropics and subtropics, the most advanced and best quality measurements of tropospheric water vapour amounts are mainly per-

AMTD

2, 1625–1662, 2009

formed at mid- and high-latitudes in countries which dispose of the necessary resources for implementing and maintaining the required sophisticated instrumentation (e.g. high resolution spectrometers) and for contracting trained personnel. There are some widely-automated water vapour measuring experiments, like Cimel sunphotometers, GPS receivers, or radiosondes, with a good global coverage (including the subtropics and tropics). The quality of the total precipitable water vapour (PWV) data produced by these automated techniques is assessed by a variety of intercomparison studies (e.g. Revercomb et al., 2003; Van Baelen et al., 2005; Sapucci et al., 2007; Bokoye et al., 2007; Alexandrov et al., 2009). Such a quality assessment is a prerequisite for applying the data for research since the expected trends in the PWV values are in the order of a few tenth of mm per decade (Trenberth et al., 2005). However, most of these intercomparison studies are limited to intensive campaign periods and none of them compares to high resolution FTIR measurements. We think that a comparison to FTIR data, which have a theoretical precision of a few percent (Schneider et al., 2006a), is important since it allows for an improved quality assessment.

In addition, water vapour is in particular effective as greenhouse gas in the middle and upper troposphere (e.g. Spencer and Braswell, 1997; Held and Soden, 2000). Thus, long-term observations of middle/upper tropospheric water vapour amounts are of particular interest for the climate change research community. However, performing precise routine water vapour measurements at these altitudes is difficult and quality assessments of free tropospheric water vapour measurements are even more limited to campaigns than PWV quality assessments (e.g. Vömel et al., 2007). We think that the long-term quality of the middle/upper tropospheric water vapour radiosonde measurements is not sufficiently documented, which hinders its use for climate research.

Ground-based high quality remote sensing experiments have the potential to observe continuously and consistently upper-air trace gases. The ground-based FTIR experiments of NDACC (Network for Detection of Atmospheric Composition Change, Kurylo, 2000) measure high quality solar absorption spectra since many years. These measurements disclose plenty of information about the distribution of many different at-

AMTD
2, 1625–1662, 2009

mospheric trace gases. They allow the measurement of precise water vapour column amounts and profiles (Schneider et al., 2006a; Schneider and Hase, 2009b). Palm et al. (2008) shows a long-term comparisons between FTIR, ground-based microwave radiometer, and satellite (sensors SCIAMCHY and AMSU-B) PWV data.

In this paper we compare PWV and water vapour profile measurements performed by a highly-sophisticated FTIR system with data obtained from globally well distributed and widely-automated techniques: Cimel sunphotometer, MFRSR, GPS receiver, and Vaisala radiosonde RS92. The study applies the most advanced FTIR water vapour inversion techniques. It is based on routine measurements made at the subtropical Izaña Atmospheric Research Centre (in Spanish letters: CIAI) covering more than four years. We document the quality and important limitations of each technique. A welcome side effect of this paper is to make the scientific community aware of CIAI's potential in developing and testing water vapor measurement techniques and in investigating the atmospheric water vapour evolution in the subtropics.

The following section presents the water vapor measurement techniques applied at CIAI. In Sect. 3 we compare the PWV amounts measured by five different techniques and discuss the observed disagreements. In Sect. 4 we compare tropospheric water vapor profiles measured routinely by the Vaisala RS92 radiosonde and the FTIR experiment and evaluate the quality of both techniques. Section 5 estimates the bias introduced in the FTIR, Cimel, and MFRSR data by its limitation to clear-sky observations. The most important results of our study are summarised in Sect. 6.

2 The water vapour instrumentation at the Izaña Atmospheric Research Centre

CIAI is located on the Canary Island of Tenerife, 300 km from the African west coast at 28°18′ N, 16°29′ W at 2370 m a.s.l. It unites a huge variety of different atmospheric measurement techniques. Among all these experiments there are five with the capability of detecting upper-air water vapour, which we briefly describe in the following. A more detailed presentation of CIAI's water vapour instrumentation is given in Romero

AMTD
2, 1625–1662, 2009

et al. (2009).

2.1 Ground-based FTIR

Izaña's FTIR activities started in March 1999. They form part of the Network for Detection of Atmospheric Composition Change (NDACC). There are about 25 ground-based FTIR experiments performed within NDACC, mostly in northern mid-latitudes and in polar regions. Over the last decades the NDACC FTIR experiments were essential for studying stratospheric ozone chemistry by providing a long-term dataset of different ozone relevant trace gases (e.g., Rinsland et al., 2003; Vigouroux et al., 2008). Due to its versatility a ground-based FTIR instrument is a key experiment of an NDACC station. It measures the spectra of the direct solar light beam applying a high resolution Fourier Transform Spectrometer. Figure 1 shows a spectrum for the 700 cm^{-1}–1350 cm^{-1} (7.4–13.5 μm) region. The bottom panel gives an impression of the huge amount of information present in these high resolution spectra. It shows two spectral microwindows with the wavenumber scale being stretched by a factor of 200. Individual rotational-vibrational lines of different absorbers (O_3, H_2O, HDO, CH_4, etc.) are discernable. The high spectral resolution allows an observation of the pressure broadening effect, i.e. the line shape depends on the pressure where the absorption takes place (compare widths of the lines of H_2O, which absorbs mainly in the lower troposphere, with the width of the lines of O_3, which absorption mainly in the stratosphere). The high resolution spectra disclose not only the total column amount of the absorber but also contain some information about its vertical distribution.

The inversion problems faced in atmospheric remote sensing are in general underdetermined and the solution has to be properly constrained. An extensive treatment of the topic is given in the textbook of C. D. Rodgers (Rodgers, 2000). During the last years the NDACC-FTIR community has increased its efforts of monitoring the tropospheric distribution of greenhouse gases, including water vapour. The inversion of atmospheric water vapour amounts from measured ground-based FTIR spectra is far from being a typical atmospheric inversion problem and, due to its large vertical gra-

dient and variability, standard retrieval methods are often not suited. During the last years, the ground-based FTIR group of the Institute for Meteorology and Climate Research (department of Trace Constituents in the Stratosphere and Tropopause Region; in German letters: IMK-ASF), Karlsruhe, Germany, developed a water vapour analysis algorithm (Hase et al., 2004; Schneider et al., 2006a,b; Schneider and Hase, 2009a). To fully exploit the capabilities of current FTIR measurements we recommend to apply the analysis method as suggested in Schneider and Hase (2009b).

2.2 Multifilter rotating shadow-band radiometer (MFRSR)

A multifilter rotating shadow-band radiometer (MFRSR) detects irradiances at CIAI since 1996. It measures at six narrow wavelength passbands between 410 nm and 940 μm the global horizontal, the diffuse horizontal, and the direct normal irradiances. The first is measured directly, whereas the latter two are calculated from a sequence of three measurements. For the middle measurement a shadowing band blocks a strip of the sky where the Sun is located and for the other two the shadowing band blocks strips of the sky 9° to either side. These side measurements permit a correction of the excess sky blocked during the middle (Sun-blocking) measurement necessary to determine the diffuse horizontal irradiances. The direct normal irradiances are than calculated by subtracting the diffuse horizontal from the global horizontal irradiances. For more details please refer to Harrison et al. (1994). The MFRSR sensors have a very good temporal and a reasonable spatial coverage, since they measure automatically at many stations of the Baseline Surface Radiation Network (BSRN; Ohmura et al., 1998).

A very critical aspect of automated radiation measurements is cloud screening. The huge amount of measurements requires the application of an automated procedure to separate cloud affected data from clear sky data. Our automated cloud screening is based on iterative Langley plots. It considers outliers as cloud affected measurements. For more details please refer to Romero et al. (2009).

The PWV is calculated from the direct normal irradiances determined for the 940 nm

passband. At Izaña we determine the water vapour columns by the modified Langley plot method. Therefore, the relation between the slant optical depth and the water vapour slant column amounts is approximated by a power law parameterisation (e.g., Bruegge et al., 1992). Uncertainties in this parameterisation and uncertainties in the Langley regression (due to variable atmospheric water vapour amounts) are the major error sources of MFRSR's water vapour data. A good overview of MFRSR's water vapour retrieval technique and the error sources is given by Alexandrov et al. (2009).

In addition we perform a data post processing to screen low quality measurements. It is similar to the method applied by Alexandrov et al. (2004) for an automated cloud screening of the MFRSR irrandiance measurements. It consists in analysing the inhomogeneity of the atmospheric water vapour field as determined by the MFRSR. Therefore, we calculate the parameter $\epsilon = 1 - \frac{\exp(\overline{\ln \mathrm{PVW}})}{\overline{\mathrm{PVW}}}$. Here the overbar indicates a moving average over one hour. For a homogeneous dataset the value of ϵ is close to 0, for an extremely inhomogeneous dataset it is close to 1. Figure 2 shows an histogram for the values of ϵ encountered in the MFRSR PVW data between 2005 and 2009. The peak at $10^{-2.7}$ represents the typical atmospheric water vapour inhomogeneity, whereas the second peak close to 1 is caused by sudden erroneous changes in the MFRSR PVW due to inefficient cloud screening, a not completely blocked Sun, incorrectly estimated total horizontal irradiances, etc. We put the threshold at an ϵ of $10^{-1.6}$, i.e. we consider that only MFRSR PVW values with $\epsilon < 10^{-1.6}$ are reliable.

2.3 Cimel sunphotometer

The Cimel sunphotometer is an automated sun and sky scanning filter radiometer. At CIAI first Cimel measurements were made in 1997 and they are continuously performed since 2004. The Cimel sunphotometer measures at 8 different passbands between 340 nm and 1020 nm. Its field of view is 1.2°. The pointing of the instrument is controlled by astronomical calculations. For the direct sun measurements the tracking is in addition assisted by a four-quadrant detector. Direct sun measurements are made

typically every 15 min. The sky is scanned at a large number of different angles with respect to the sun, which allows to determine many different aerosol properties (theory of Mie scattering). The Cimel measurements are performed at several hundred globally distributed sites within AERONET (Aerosol Robotic Network, Holben et al., 1998). As for the MFRSR, the Cimel PWV is calculated from the 940 nm passband direct sun observations applying the modified Langley technique (Schmid et al., 2001). In this paper we use AERONET level 1.5 data, which are automatically cloud screened by a method described in Smirnov et al. (2000). Romero et al. (2009) shows that there is no significant difference between the Cimel PWV AERONET level 1.5 and level 2.0 data.

2.4 GPS receiver

Due to refraction in the atmosphere the radio signals emitted by the GPS (or GLONASS) satellites are delayed. The Zenith Total Delay (ZTD) is the sum of the Zenith Hydrostatic Delay (ZHD) associated to induced dipole moments of the atmospheric molecules and the Zenith Wet Delay (ZWD) associated to the permanent dipole moments of the water vapour molecules. Absolute ZTD values can only be determined if the GPS receiver is operated within a network of reasonable spatial coverage (the same satellite must be seen at different GPS stations from different elevation angles, Duan et al., 1996). At CIAI we apply a Leica GRX 1200GG pro GPS/GLONASS receiver, which is operated within the European EUREF network (Bruyninx, 2004). The CIAI GPS instrument is property of the Spanish National Geographic Institute (in Spanish: Instituto Geográfico Nacional, IGN), which provides us with 15 min means ZTD values. They are calculated applying the Bernese software (Rothacher, 1992).

We separate the ZHD and ZWD (the amount of interest). The ZHD can be easily predicted if the surface pressure is known. It is typically one order of magnitude larger than the ZWD, and consequently precise measurements of surface pressure are essential for a ZWD determination. The ZWD is then converted in PWV using the refraction constants of water vapour (for more details please refer to Romero et al., 2009).

Ground-based GPS measurements offer a good global coverage (IGS (International

GNSS service) network, Dow et al., 2005) and can provide a valuable dataset for climate research (Wang et al., 2007).

2.5 Meteorological radiosonde (Vaisala RS92)

On Tenerife Island meteorological ptu-sondes are launched automatically twice daily (at 11:15 UT and 23:15 UT) since the 1970s, from a site situated at the cost line, approximately 15 km to the south of CIAI (WMO station #60018). Until June 2005 the Vaisala RS80 radiosonde was applied as operational ptu sonde. Since then the Vaisala RS92 sondes are used. We correct the temperature and radiation dependence (in the case of daytime soundings) of the RS92 sensor as suggested by Vömel et al. (2007). Then their precision is estimated to be better than 20% for altitudes below 15 km. The Vaisala RS92 radiosonde is applied at many sites throughout the globe within WMO's upper air meteorological network.

3 Comparison of the PWV data

We compare data measured since 2005, when the last major changes of Izaña's water vapour instrumentation took place: In the beginning of 2005 the Bruker FTS 120M was replaced by a Bruker 120HR and in June 2005 the Vaisala RS92 sonde replaced the RS80 as operational radiosonde. As temporal coincidence criterion for the comparisons we use one hour, i.e. we only compare measurements that are performed within one hour. The definition of this coincidence criterion is straight forward when comparing the remote sensing measurements of Cimel, MFRSR, GPS, and FTIR, since their measurements take only some seconds (Cimel, MFRSR) or less than 15 min (GPS, FTIR). When there is more than one pair of measurement that fulfills this criterion we exclusively choose the pair with the minimal time difference. Concerning the radiosonde measurements the situation is different. These measurements take approx. one hour (time needed until sonde reaches 15 km). In this case we take the time when the sonde

reaches 4 km (1.63 km above Izaña) as reference time for the one hour temporal coincidence criterion, since the layer between the altitude of Izaña and the altitude of 4 km concentrates typically 50% of all the water vapour column above Izaña.

3.1 Time series of PWV data

The upper panel of Fig. 3 depicts a time series of the total water column above Izaña as measured by the ground-based FTIR since 2005. On dry days the water vapour column is smaller than 0.5 mm and on wet days it reaches 20 mm, i.e. the variability spans practically two orders of magnitude, which is a typical characteristic of atmospheric water vapour amounts. The remaining panels of Fig. 3 depict the time series of the differences between the FTIR data and the data measured simultaneously by the other experiments. This figure gives a good overview of the availability of data from the different experiments: The Cimel data are available continuously since 2005 with the exception of the period from April to September 2008, where there are only version 1.0 (not cloud screened) data in the database. The MFRSR data are available continuously since 2005 with some smaller periods without data in 2005. The RS92 sonde is the operative meteorological sonde since June 2005, and provides data twice daily. Finally, the GPS receiver was installed in spring 2008 and provide data continuously since mid July 2008. We observe that Cimel, MFRSR, GPS, and RS92 agree well with the FTIR and that there is no trend in the difference. However, concerning the MFRSR (third panel from the top) we observe an annual cycle in the difference to the FTIR. The difference is especially large and positive (MFRSR overestimates FTIR values) in summer, and close to zero in winter. Concerning the Cimel, we observe no annual cycle but occasionally an accumulation of outliers (March/April 2006, May 2007, and December/January 2007/08 and 2008/09).

AMTD
2, 1625–1662, 2009

3.2 Correlations between the PWV datasets

Figure 4 shows the correlations for all the data that fulfill the one hour coincidence criterion. We choose a logarithmic scale due to the large variability of the water vapour amounts. The total water vapour amounts span two orders of magnitude, are quite well log-normally distributed, and consequently a presentation on a logarithmic scale is more adequate than a presentation on a linear scale. A linear scale presentation would give too much weight to the rarely occurring large water vapour amounts, whereas a log-scale presentation adequately reveals how the different techniques get along with the huge dynamic range of atmospheric water vapour amounts. Cimel, MFRSR, and GPS measure with a frequency of several seconds, which explains the large number of coincidences for comparisons which involves these data (although GPS is only operating since July 2008). Generally the data of the different sensors correlate quite well. The correlation coefficient ρ is above 0.92 (with the exception of the GPS versus Cimel correlation where ρ is 0.845). For all instruments the correlation is the best with the FTIR data. Whenever FTIR data is involved the respective correlation coefficient ρ is above 0.95. Among the correlation that do not involve FTIR data, only the correlation between Cimel and MFRSR and between Cimel and RS92 leads to a coefficient ρ above 0.95. All correlations with the GPS data show increased scatter for low water vapour amounts. Furthermore, then the GPS technique tends to underestimate the water vapour amounts. On the other hand, for large water vapour amounts the scatter is small. The GPS data seem to be more precise for high water amounts than for low water amounts. This issue is examined in more detail in the last paragraph of this section. The relatively poor correlation between GPS and Cimel (ρ of 0.853) seems at first glance in contradiction to the good correlation of the FTIR to both the GPS and Cimel (ρ of 0.958 and 0.986, respectively). There are two reasons for this poor correlation. Firstly, GPS and Cimel measurements only coincide between October 2008 and January 2009, in a relatively short period, in which low water vapour amounts prevail. As aforementioned, the GPS data seems to be less precise for low water amounts. The

AMTD
2, 1625–1662, 2009

comparison between GPS and Cimel is restricted to a period when GPS data is of relatively low quality. The comparison of FTIR with GPS includes a large number of days between July 2008 and January 2009. It covers a wide range of atmospheric water vapour content and the presumed deficiencies of the GPS systems in measuring low water amounts are less discernible. Secondly, the Cimel technique measures visible and near infrared radiation, which is absorbed by clouds. The measurements which are affected by clouds have to be sorted out, which is done automatically by the cloud screening algorithm of Smirnov et al. (2000). The radio signals analysed by the GPS are not affected by clouds and, consequently, the quality of the comparison between GPS and Cimel depends strongly on the effectiveness of Cimel's cloud screening algorithm. In contrast, the comparison between Cimel and FTIR data is a reliably cloud screened comparison, since the FTIR measurements are performed manually and only in the absence of clouds. The comparison between FTIR and Cimel is independent on the effectiveness of Cimel's cloud screening algorithm.

Table 1 resumes the comparisons and gives mean and standard deviation of the mean values for the differences between the experiments, i.e. it informs about the systematic differences and the scatter between the different measurement techniques. The values are given in absolute water amount (in mm) and in percent. Again, it reveals that the lowest scatter is achieved when FTIR data are involved. Interesting is the very small systematic difference between FTIR and GPS. Given the large number of coincidences (more than 100) this observation is a very robust evidence of a surprisingly good agreement between the water vapour scales of the GPS technique, which is based on radio signals, and the infrared-based FTIR technique.

Table 1 collects the mean difference and scatter between two coinciding measurements. For every comparison (e.g. FTIR versus Cimel, FTIR versus RS92, FTIR versus GPS, etc.) a different ensemble of coincidences is applied. In addition we can perform the comparisons applying a unique ensemble and thereby reduce the influence of varying atmospheric conditions . The three independent experiments FTIR, RS92, and Cimel coincide on 158 days within 1 h. The comparison based on this en-

semble confirms the results of Table 1: the smallest scatter is found when FTIR data are involved (FTIR versus RS92: ±15.2%, FTIR versus RS92: ±14.4%, and RS92 versus Cimel: ±21.1%). The root-square-sum of the scatter FTIR versus RS92 and FTIR versus Cimel ($\sqrt{15.2^2+14.4^2}$%=20.9%) is smaller than the scatter RS92 versus Cimel indicating the high precision of the FTIR PWV data. We conclude that the precision of the FTIR PWV data is in the sub percent range and that the scatter values as given in Table 1 for comparisons to the FTIR PWVs are a good estimation of the precision of the Cimel and MFRSR data. The scatter FTIR versus RS92 and FTIR versus GPS, as given in Table 1, are due to a combination of uncertainties in the RS92 and GPS measurements and the detection of different airmasses. They represent upper limits of the RS92 and GPS uncertainties.

3.3 Dependence of the PWV data quality on observation geometry and atmospheric conditions

The signal imprinted by atmospheric water vapour on the radiances measured by the FTIR, Cimel, and MFRSR instruments is the stronger the larger the water vapour slant column amount, which potentially results in a water vapour slant column dependency of their precision. The water vapour slant column amount is the atmospheric vertical water vapour amount multiplied by the inverse of the sine of the elevation angle under which the observation is performed, i.e. it strongly depends on the observation geometry. The FTIR observes at all elevation angles above a few degrees, however, the majority of the observations are made at elevation angles above 30°. Cimel and MFRSR, measure in general quasi-continuously during the whole day. The potential dependency on the slant column amount can be estimated by plotting the differences between the FTIR, Cimel and MFRSR data versus the water vapour slant column amount (see Fig. 5). The difference between Cimel and MFRSR show the largest dependency on the water vapour slant column amounts, which allows the conclusion that the slant column dependence of Cimel-FTIR and MFRSR-FTIR is mainly due to the Cimel and MFRSR

data. This suggests that the FTIR data are practically independent on the water vapour slant column amount. Even for low slant columns the FTIR data are very precise and we can apply the FTIR data to estimate how the Cimel and MFRSR data depend on the water vapour slant column amount (first two panels from the left of Fig. 5). We find that for slant column amounts above 7.5 mm the scatter between Cimel and FTIR data reduces to ±6.7% compared to ±12.7% as listed in Table 1 for the whole ensemble. The quality of the MFRSR data is also the better the larger the slant column amounts. If we limit to amounts above 7.5 mm the scatter between FTIR and MFRSR is reduced to ±11.0% compared to ±17.2% for the whole ensemble.

As aforementioned for very dry conditions the GPS system underestimates the atmospheric water vapour content. This is illustrated in Fig. 6, which plots the difference between GPS and FTIR data versus PWV. However, the GPS technique works very reliable for amounts above approximately 3.5 mm, which thus can be considered as detection limit of the GPS experiment. If we only consider measurements with total column amounts above this detection limit the GPS data is of good quality. Then the agreement with the FTIR data is (−0.1±9.9)% (compared to (−5.4±19.5)% as listed in Table 1 for the whole ensemble). Such an increased relative uncertainty of the GPS PWVs for very low atmospheric water vapour amounts is expectable, since it is obtained by subtracting two values of similar magnitude (the targeted ZWD is the difference between the ZTD and the ZHD). For low water vapour amounts the ZTD is almost completely due to the ZHD. Then small relative errors in these amounts produce a large relative error in their difference (the ZWD).

Both RS92 and GPS measure during day and night and we analyse if there are differences between the day- and nighttime measurements. During the day the RS92 measures typically 12.7% more PWV than the GPS, whereas we find no significant systematic difference between RS92 and GPS in the nighttime measurements. The daytime wet bias, as observed in the RS92 data, is caused by a too strong radiation correction (we performed this correction according to Vömel et al., 2007). For more details please refer to Sect. 5.

AMTD
2, 1625–1662, 2009

4 Comparison of vertical profiles

Here we compare water vapour profiles measured routinely at CIAI by two different techniques: the Vaisala RS92 in-situ sensor and the ground-based FTIR system. The latter technique only provides reasonable water vapour profiles if the developments of the IMK-ASF water vapour analysis algorithm are applied (Schneider and Hase, 2009b).

When comparing remotely-sensed vertical distribution profiles with in-situ measured profiles it is important to account for the inherent vertical resolution of the remotely-sensed data. The averaging kernels document the vertical structures that are detectable by the remote sensing measurement. A typical FTIR averaging kernel for water vapour when applying the IMK-ASF inversion algorithm is shown in Fig. 7. The FTIR system is able to detect 2 km thick layers in the lower troposphere, 3–4 km layers in the middle troposphere, and 6 km layers in the upper troposphere. The averaging kernels for 3, 5, and 8 km (representative for the lower, middle and upper troposphere) are highlighted in Fig. 7 by red, blue and green colors, respectively. For an adequate comparison we have to adjust the vertical resolution of the vertically highly-resolved data to the vertically poorly-resolved data. In our case the vertically highly resolved RS92 in-situ profiles x_{RS92} have to be degraded towards the vertically moderately resolved FTIR profiles. This is done by a convolution with the FTIR averaging kernels $\hat{\mathbf{A}}$:

$$\hat{x}_{\mathrm{RS92}} = \hat{\mathbf{A}}(x_{\mathrm{RS92}} - x_a) + x_a \quad (1)$$

The result is a smoothed RS92 profile ($\hat{x}_{\mathrm{RS92}}$) with the same vertical resolution as the FTIR profile.

For the profile comparison we slightly relaxed our one hour coincidence criterion. Here we consider as coincidence if the FTIR measures within one hour to the sonde located anywhere between 2.37 km (CIAI's altitude level) and 15 km. This coincidence criterion increases the number of coincidences if compared to Figs. 3, 4, and Table 1 from 195 to 246, since the sonde needs about one hour to reach 15 km. The Figs. 8–10

AMTD
2, 1625–1662, 2009

depict time series of data that fulfill this coincidence criterion. The upper panels show the water vapour mixing ratios as measured by the FTIR and the bottom panels the relative differences between FTIR and RS92. The altitudes of 3 km, 5 km, and 8 km represent the lower, middle, and upper troposphere. These are the altitudes whose typical averaging kernels are highlighted in Fig. 7 by red, blue and green colors. In the lower troposphere (Fig. 8) the mixing ratios measured in coincidence vary between 0.025% and 1.2%, i.e. cover almost two orders of magnitude and are well representative for the huge atmospheric water vapour variability. As a mean the FTIR overestimates the RS92 values by 23.5%. The scatter between FTIR and RS92 is 28.8%. The coincident measurements of the mixing ratios of middle tropospheric water vapour (Fig. 9) vary between 0.01% and 0.6%. The mean difference and scatter between the FTIR and RS92 data is (−15.1±23.3)%. If compared to the lower troposphere the scatter is reduced by more than 5%. The scatter is partly due to the detection of different airmasses (the RS92 detects the airmass at the sonde's location and the FTIR the airmass between the spectrometer and the Sun). We think that the reduced scatter reflects the larger stability of the middle tropospheric water vapour fields if compared to the more variable lower tropospheric fields. In the upper troposphere (Fig. 10) the mixing ratios within the ensemble of coincident measurements vary between 0.004% and 0.12%. The mean difference and scatter is (−1.8±20.6)%. The scatter is further reduced if compared to lower and middle troposphere, indicating a further reduction of temporal and spatial water vapour variabilities at these altitudes.

The agreement between the RS92 and FTIR profiles is very satisfactory. Their water vapour mixing ratios, which cover a dynamic range of two orders of magnitude, agree within 20%. The higher scatter between FTIR and RS92 at lower altitudes can be explained by the detection of different airmasses and an increased spatial and temporal variability in the lower troposphere. Vömel et al. (2007) estimated a precision of 20% for the RS92 mixing ratios, which suggests that most of the scatter observed in our intercomparison is due to RS92 uncertainties. We conclude that the FTIR technique offers very precise tropospheric water vapour profiles, with a vertical resolution of 2, 4,

AMTD
2, 1625–1662, 2009

and 6 km in the lower, middle and upper troposphere, respectively.

We observe no tendency in the difference between FTIR and RS92, which documents the feasibility of both techniques for studying the long-term evolution of the vertical distribution of tropospheric water vapour. This is in particular true for the FTIR technique. Highly-resolved infrared solar absorption spectra are measured since more than two decades at a variety of globally distributed sites. These measurements are less influenced by a change in the experimental instrumentation than the sonde in-situ measurements. The sonde sensors have changed several times during the last decades and it is not clear how this will affect time series produced from these measurements. On the other hand, reprocessing the historic FTIR measurements applying the new retrieval developments would provide a consistent long-term time series.

5 Bias of clear-sky observations

The FTIR, Cimel, and MFRSR only provide water vapour data if the line between the instrument and the Sun is cloud free. It seems likely that this restriction produces a dry bias of the FTIR, Cimel and MFRSR water vapour data. Such a potential clear sky bias is an important drawback of many water vapour remote sensing techniques and it is important when interpreting visible and infrared space-based water vapour observations (e.g. Lanzante and Gahrs, 2000). Gaffen and Elliot (1993) estimated the clear sky dry bias from a set of radiosonde observations performed in the period 1988–1990 at 15 different Northern Hemispheric site. They found a significant dry bias, which strongly depends on latitude. It reaches +50% at high latitudes, whereas it is below +10% for the tropics. They defined the dry bias B as:

$$B = 1 - \frac{\overline{PWV_c}}{\overline{PWV_a}} \quad (2)$$

Here the overbar indicates mean values and PWV_a are all PWV values and PWV_c those obtained at clear-sky conditions.

AMTD
2, 1625–1662, 2009

We calculate the dry bias (B) of CIAI's FTIR, Cimel, and MFRSR measurements with PWV_c being the PWV value measured by the RS92 sonde when it coincides with a FTIR, Cimel, or MFRSR measurement. The B values for each instrument are listed in Table 2. DJF, MAM, JJM, and SON represent ensembles for winter (December, January, and February), spring (March, April, and May), summer (June, July, and August), and autumn (September, October, and November), respectively. The row "year" shows all-season values. The different ensembles are sufficiently large for a reliable estimation of B (the smallest ensemble is the DJF FTIR ensemble which consists of 33 RS92 observations). The Cimel and, in particular, the FTIR PWV data have a significant dry bias. It is larger in winter than in summer. This is in good agreement to the latitudinal dependence as observed by Gaffen and Elliot (1993), since in winter CIAI's atmosphere has mid-latitudinal and in summer subtropical characteristics. A seasonality is also observed in the MFRSR B values. However, the MFRSR bias is not significant. There is a dry bias in winter, but in summer the MFRSR PWV data are wet-biased. A reason might be that high aerosol loadings in summer, which are correlated to a particularly dry atmosphere, are sorted out by the MFRSR cloud or post processing data screening. Like the RS92, the GPS instrument also measures at cloudy sky conditions. The FTIR, Cimel, and MFRSR PWV dry bias estimated from GPS measurements is similar to the dry bias biased on RS92 measurements, however, it is less reliable since the GPS analysis is only possible for a 8 months period.

The RS92 measurements allow for an estimation of vertical profiles of the dry bias. Figure 11 shows the profiles of the FTIR dry bias. In particular in summer there is a slight maximum dry bias around 8 km. Except for winter, the dry bias decreases rapidly above 10 km. Generally it is insignificant above 12 km.

In addition we examine the known daytime dry bias of the RS92 measurements (it is nearly one order of magnitude smaller than the clear sky bias of the FTIR measurements). After applying a temperature and radiation correction as suggested by Vömel et al. (2007) we observe a daytime wet bias in the RS92 PWV data of about −3% (de-

AMTD
2, 1625–1662, 2009

fined as $1-\frac{\overline{PWV_{day}}}{\overline{PWV_{day+night}}}$). We do not detect a clear daytime bias in the GPS data and think that this bias is due to a too strong radiation correction of the daytime measurements. This supposition is supported by the altitude dependence of this wet bias. It is rapidly increasing above 10 km. If we remove the radiation correction we observe the known daytime dry bias in the PWV data of about +4%, which is also altitude dependent (+3% in the lower troposphere and +10% at 10 km). The radiation correction of Vömel et al. (2007) was determined for a tropical site. At Izaña the RS92 radiation correction should be weaker.

6 Conclusions

We performed an extensive long-term intercomparison of five different upper-air water vapour measurement techniques (FTIR, Cimel, MFRSR, GPS, and RS92) conducted continuously at the Izaña Atmospheric Research Centre. All five techniques are able to measure the total precipitable water vapour (PWV) amount. In addition, the FTIR and RS92 experiments measure vertical distribution profiles between the Research Centre and an altitude of approx. 15 km.

The FTIR, Cimel, MFRSR, and RS92 measurements are performed since 2005, and we observe no significant trend between their total column amounts. The FTIR technique provides the most precise data. We empirically estimate a precision of better than 1%. We found that both the Cimel and the MFRSR precision depends on the slant column amounts. For slant column amounts above 7.5 mm the Cimel and MFRSR data are of good quality. Then their precision is about 7% and 11%, respectively, whereas for very low slant column amounts ($\leq$2 mm) their precision is only about 25%. We think that the automatic cloud screening routine applied to the Cimel version 1.5 data not completely removes cloud affected measurements. A post processing of Cimel's PWV data for screening low quality data (as we did for the MFRSR data, Fig. 2) would further improve this precision. Concerning the GPS data we found a detection limit

of 3.5 mm. For water vapour column amounts above this limit the GPS data quality is good (precision of better than 10%), whereas for lower column amounts the GPS systematically underestimates the real values. The empirically estimated PWV precisions are collected in Table 3. The uncertainty values given for GPS and RS92 are upper limits, since both instruments detect different airmasses as the FTIR instrument.

A very positive surprise of our study is the small bias between the FTIR and GPS data. Both experiments are based on different principles (passive, active remote sensing). Nevertheless, we can demonstrate with high confidence, due to the large number of coincidences, that systematic differences between them are almost negligible. A combined FTIR/GPS sensor would be a very promising development. It could provide high quality data for cloudy as well as extremely dry condition and during day and night.

Precise routine measurements of tropospheric water vapour profiles are difficult, but very important for climate change research. The comparison of RS92 and FTIR profile measurements documents that both techniques provide valuable data for investigating the long-term evolution of the middle/uppere tropospheric water vapour amounts. However, radiosondes only apply the RS92 humidity sensor since 2004/2005, and the restriction to four or five years of data limits its use for trend analyses. On the other hand, high resolution solar absorption spectra are measured since many years by NDACC's ground-based FTIR experiments (at some stations since more than two decades). Reprocessing the historic measurements applying recent inversion algorithm developments would produce a consistent long-term data set of lower, middle, and upper tropospheric water vapour amounts.

It is important to be aware of the significant dry bias of visible and infrared remote sensing techniques caused by the restriction to clear sky conditions. This dry bias has to be considered when applying the FTIR, Cimel, and MFRSR data for research.

Acknowledgements. The FTIR activities are supported by the European Commission and the Deutsche Forschungsgemeinschaft by funding via the projects SCOUT-O3 and GEOMON (contract SCOUT-O3-505390 and GEOMON-036677) and RISOTO (Geschäftszeichen SCHN 1126/1-1), respectively. We would like to thank the Instituto Geográfico Nacional (IGN) for pro-

viding the GPS/GLONASS Zenith Total Delay data. We are grateful to the Goddard Space Flight Center for providing the temperature and pressure profiles of the National Centers for Environmental Prediction via the automailer system.

References

Alexandrov, M. D., Marshak, A., Cairns, B., Lacis, A. A., and Carlson, B. E.: Automated cloud screening algorithm for MFRSR data, Geophys. Res. Lett., 31(4), L04118, doi:10.1029/2003GL019105, 2004. 1631

Alexandrov, M. D., Schmid, B., Turner, D. D., Cairns, B., Oinas, V., Lacis, A. A., Gutman, S. I., Westwater, E. R., Smirnov, A., and Eilers, J.: Columnar water vapor retrievals from multifilter rotating shadowband radiometer data, J. Geophys. Res., 114, D02306, doi:10.1029/2008JD010543, 2009. 1627, 1631

Bokoye, A. I., Royer, A., Cliche, P., and O'Neill, N.: Calibration of Sun RadiometerBased Atmospheric Water Vapor Retrievals Using GPS Meteorology, J. Atmos. Oceanic Technol., 24, 964–979, 2007. 1627

Bruegge, C. J., Conel, J. E., Green, R. O., Margolis, J. S., Holm, R. G., and Toon, G.: Water vapor column abundances retrievals during FIFE, J. Geophys. Res., 97, 18759–18768, 1992. 1631

Bruyninx, C.: The EUREF Permanent Network: a multi-disciplinary network serving surveyors as well as scientists, GeoInformatics, 7, 32–35, 2004. 1632

Dow, J. M., Neilan, R. E., and Gendt, G.: The International GPS Service (IGS): Celebrating the 10th Anniversary and Looking to the Next Decade, Adv. Space Res., 36, 320–326, doi:10.1016/j.asr.2005.05.125, 2005. 1633

Duan, J., Bevis, M., Fang, P., Bock, Y., Chiswell, S., Businger, S., Rocken, C., Solheim, F., van Hove, T., Ware, R., McClusky, S., Herring, T. A., and King, R. W.: GPS Meteorology: Direct Estimation of the Absolute Value of Precipitable Water, J. Appl. Meteor., 35, 830–838, 1996. 1632

Gaffen, D. J. and Elliot, W. P.: Column Water Vapor Content in Clear and Cloudy Skies, J. Climate, 6, 2278–2287, 1993. 1641, 1642

Harrison, L., Michalsky, J., and Berndt, J.: Automated multifilter rotating shadow-band radiome-

ter: an instrument for optical depth and radiation measurements, Appl. Optics, 33, 5118–5125, 1994. 1630

Hase, F., Hannigan, J. W., Coffey, M. T., Goldman, A., Höpfner, M., Jones, N. B., Rinsland, C. P., and Wood, S. W.: Intercomparison of retrieval codes used for the analysis of high-resolution, ground-based FTIR measurements, J. Quant. Spectrosc. Ra., 87, 25–52, 2004. 1630

Held, I. M. and Soden, B. J.: Water Vapour Feedback and Global Warming, Annu. Rev. Energy Environ., 25, 441–475, 2000. 1626, 1627

Holben, B. N., Eck, T. F., Slutsker, I., Tanré, D., Buis, J. P., Setzer, A., Vermote, E., Reagan, J. A., Kaufman, Y. J., Nakajima, T., Lavenu, F., Jankowiak, I., and Smirnov, A.: AERONET – A Federated Instrument Network and Data Archive for Aerosol Characterization, Rem. Sens. Environ., 66, 1–16, 1998. 1632

Kurylo, M. J. and Zander, R.: The NDSC – Its status after 10 years of operation, Proceedings of XIX Quadrennial Ozone Symposium, Hokkaido University, Sapporo, Japan, 167–168, 2000. 1627

Lanzante, J. R. and Gahrs, G. E.: The "Clear-Sky Bias" of TOVS Upper-Tropospheric Humidity, J. Climate, 13, 4034–4041, 2000. 1641

Ohmura, A., Gilgen, H., Hegner, H., Müller, G., Wild, M., Dutton, E. G., Forgan, B., Fröhlich, C., Philipona, R., Heimo, A., König-Langlo, G., McArthur, B., Pinker, R., Whitlock, C. H., and Dehne, K.: Baseline Surface Radiation Network (BSRN/WCRP): New Precision Radiometry for Climate Research, B. Am. Meteorol. Soc., 79, 2115–2136, 1998. 1630

Palm, M., Melsheimer, C., Noël, S., Notholt, J., Burrows, J., and Schrems, O.: Integrated water vapor above Ny Ålesund, Spitsbergen: a multisensor intercomparison, Atmos. Chem. Phys. Discuss., 8, 21171–21199, 2008, http://www.atmos-chem-phys-discuss.net/8/21171/2008/. 1628

Pierrehumbert, R. T.: Thermostats, Radiator Fins, and the Local Runaway Greenhouse, J. Atmos. Sci., 52, 1784–1806, 1995. 1626

Pierrehumbert, R. T.: Subtropical water vapor as a mediator of rapid global climate change, in: Clark PU, Webb RS and Keigwin LD eds, Mechanisms of global change at millennial time scales, American Geophysical Union Geophysical Monograph Series, 2000. 1626

Revercomb, H. E., Turner, D. D., Tobin, D. C., Knuteson, R. O., Feltz, W. F., Barnard, J., Bösenberg, J., Clough, S., Cook, D., Ferrare, R., Goldsmith, J., Gutman, S., Halthore, R., Lesht, B., Liljegren, J., Linné, H., Michalsky, J., Morris, V., Porch, W., Richardson, S., Schmid, B., Splitt, M., van Hove, T., Westwater, E., and Whiteman, D.: The ARM pro-

gram's water vapor intensive observation periods: Overview, initial accomplishments, and future challenges, B. Am. Meteorol. Soc., 84, 217–236, 2003. 1627

Rinsland, C. P., Mahieu, E., Zander, R., Jones, N. B., Chipperfield, M. P., Goldman, A., Anderson, J., Russell III, J. M., Demoulin, P., Notholt, J., Toon, G. C., Blavier, J.-F., Sen, B., Sussmann, R., Wood, S. W., Meier, A., Griffith, D. W. T., Chiou, L. S., Murcray, F. J., Stephen, T. M., Hase, F., Mikuteit, S., Schultz, A., and Blumenstock, T.: Long-Term Trends of Inorganic Chlorine from Ground-Based Infrared Solar Spectra: Past Increases and Evidence for Stabilization, J. Geophys. Res., 108(D8), 4252, doi:10.1029/2002JD003001, 2003. 1629

Rothacher, M.: Orbits of satellite systems in space goedesy, Ph.D. thesis, University of Bern, Bern, Switzerland, 1992. 1632

Rodgers, C. D.: Inverse Methods for Atmospheric Sounding: Theory and Praxis, World Scientific Publishing Co., Singapore, ISBN 981-02-2740-X, 2000. 1629

Romero, P. M., Cuevas, E., Ramos, R., and Schneider, M.: Programa de vapor de agua en columna del Centro de Investigación Atmosférico de Izaña: Análisis e Intercomparación de diferentes Técnicas de Medidia, NTD CIAI-1, Agencia Estatal de Meteorología, Ministerio de Medio Ambiente, y Medio Rural y Marino, NIPO: 784-09-009-9, 2009. 1628, 1630, 1632

Sapucci, L. F., Machado, L. A. T., Monico, J. F. G., and Plana-Fattori, A.: Intercomparison of Integrated Water Vapor Estimates from Multisensors in the Amazonian Region, J. Atmos. Oceanic Technol., 24, 1880–1894, 2007. 1627

Schmid, B., Michalsky, J. J., Slater, D. W., Barnard, J. C., Halthore, R. N., Liljegren, J. C., Holben, B. N., Eck, T. F., Livingston, J. M., Russell, P. B., Ingold, T., and Slutsker, I.: Comparison of columnar water-vapor measurements from solar transmittance methods, Appl. Optics, 40, 1886–1896, 2001. 1632

Schneider, M., Hase, F., and Blumenstock, T.: Water vapour profiles by ground-based FTIR spectroscopy: study for an optimised retrieval and its validation, Atmos. Chem. Phys., 6, 811–830, 2006a, http://www.atmos-chem-phys.net/6/811/2006/. 1627, 1628, 1630

Schneider, M., Hase, F., and Blumenstock, T.: Ground-based remote sensing of HDO/H_2O ratio profiles: introduction and validation of an innovative retrieval approach, Atmos. Chem. Phys., 6, 4705–4722, 2006b, http://www.atmos-chem-phys.net/6/4705/2006/. 1630

Schneider, M. and Hase, F.: Improving spectroscopic line parameters by means of atmospheric spectra: Theory and example for water vapour and solar absorption spectra, J. Quant. Spec-

trosc. Radiat. Transfer, in press, doi:10.1016/j.jqsrt.2009.04.011, 2009. 1630
Schneider, M. and Hase, F.: Reviewing the development of a ground-based FTIR water vapour profile analysis, Atmos. Meas. Tech. Discuss., 2, 1221–1246, 2009, http://www.atmos-meas-tech-discuss.net/2/1221/2009/. 1628, 1630, 1639
Smirnov, A., Holben, B. N., Eck, T. F., Dubovik, O., and Slutsker, I.: Cloud screening and quality control algorithms for the AERONET database, Rem. Sens. Environ., 73, 337-349, 2000. 1632, 1636
Spencer, R. W. and Braswell, W. D.: How Dry is the Tropical Free Troposphere? Implications for Global Warming Theory, B. Am. Meteorol. Soc., 78, 1097–1106, 1997. 1627
Trenberth, K. E., Fasullo, J., and Smith, L.: Trends and variability in column-integrated atmospheric water vapour, Clim. Dynam., 24, 741–758, 2004. 1627
Van Baelen, J., Aubagnac, J.-P., and Dabas, A.: Comparison of Near-Real Time Estimates of Integrated Water Vapor Derived with GPS, Radiosonde, and Microwave Radiometer, J. Atmos. Oceanic Technol., 22, 201–210, 2005. 1627
Vigouroux, C., De Mazière, M., Demoulin, P., Servais, C., Hase, F., Blumenstock, T., Kramer, I., Schneider, M., Mellqvist, J., Strandberg, A., Velazco, V., Notholt, J., Sussmann, R., Stremme, W., Rockmann, A., Gardiner, T., Coleman, M., and Woods, P.: Evaluation of tropospheric and stratospheric ozone trends over Western Europe from ground-based FTIR network observations, Atmos. Chem. Phys., 8, 6865–6886, 2008, http://www.atmos-chem-phys.net/8/6865/2008/. 1629
Vömel, H., Selkirk, H., Miloshevich, L., Valverde, J., Valdés, J., Kyrö, E., Kivi, R., Stolz, W., Peng, G., and Diaz, J. A.: Radiation dry bias of the Vaisala RS92 humidity sensor, J. Atmos. Oceanic Technol., 24, 953–963, 2007. 1627, 1633, 1638, 1640, 1642, 1643
Wang, J., Zhang, L., Dai, A., Van Hove, T., and Van Baelen, J.: A near-global, 2-hourly data set of atmospheric precipitable water from ground-based GPS measurements, J. Geophys. Res., 112, D11107, doi:10.1029/2006JD007529, 2007. 1633

Table 1. Results of intercomparison of different sensors: Number of coincidences (N), mean difference and standard deviation of difference in mm, and mean difference and standard deviation of difference in % ($2\times(y-x)/(x+y)$).

	FTIR	Cimel	MFRSR	GPS	RS92 (night)
Cimel	N=677 (−1.13±0.74) mm (−25.4±12.7)%				
MFRSR	N=603 (+2.85±2.05) mm (+38.2±17.2)%	N=17 951 (+3.73±2.68) mm (+62.2±17.5)%			
GPS	N=112 (−0.09±0.73) mm (−5.36±19.5)%	N=1464 (+0.42±0.96) mm (+9.49±33.9)%	N=2002 (−3.58±2.29) mm (−36.9±22.9)%		N=155 (−0.19±1.06) mm (−0.60±30.4)%
RS92 (day)	N=195 (+0.06±0.72) mm (−3.33±15.5)%	N=675 (+1.23±1.34) mm (+24.3±22.8)%	N=696 (−2.36±1.86) mm (−35.4±25.4)%	N=152 (+0.66±1.18) mm (+12.7±31.2)%	

AMTD
2, 1625–1662, 2009

Table 2. Dry bias in PWV of FTIR, Cimel, and MFRSR observations determined from RS92 measurements (expressed as $1-\frac{\overline{PWV_c}}{\overline{PWV_a}}$).

	FTIR	Cimel	MFRSR
DJF	+30.4%	+25.5%	+9.8%
MAM	+18.0%	+11.5%	+1.6%
JJA	+10.0%	−1.9%	−10.2%
SON	+14.8%	+6.6%	−3.7%
year	+11.9%	+5.6%	−4.8%

AMTD
2, 1625–1662, 2009

Table 3. Empirical estimation of the PWV data precision.

	precision	comment
FTIR	<1%	–
Cimel	13%	for slant PWV >7.5 mm: 7%
MFRSR	17%	for slant PWV >7.5 mm: 11%
GPS	<20%	for PWV > 3.5 mm: <10%
RS92	<16%	–

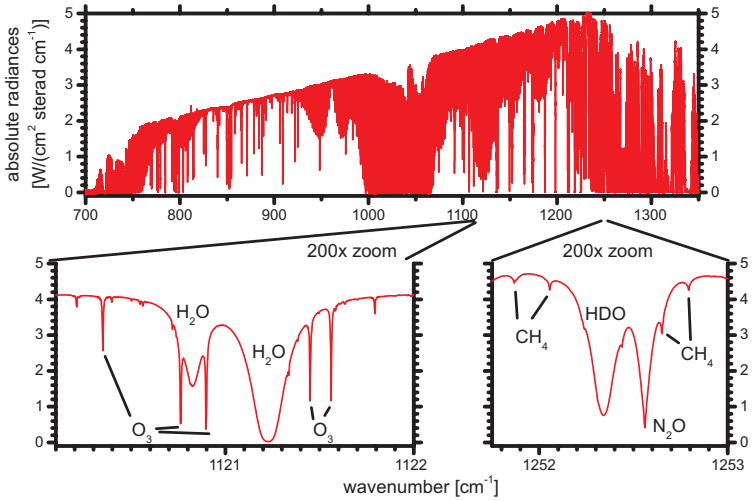

Fig. 1. Upper panel: Spectrum measured by the Fourier Transform Spectrometer with the 700–1350 cm^{-1} filter setting. Bottom panels: Zoomed out spectral microwindows containing H_2O and HDO signatures.

AMTD
2, 1625–1662, 2009

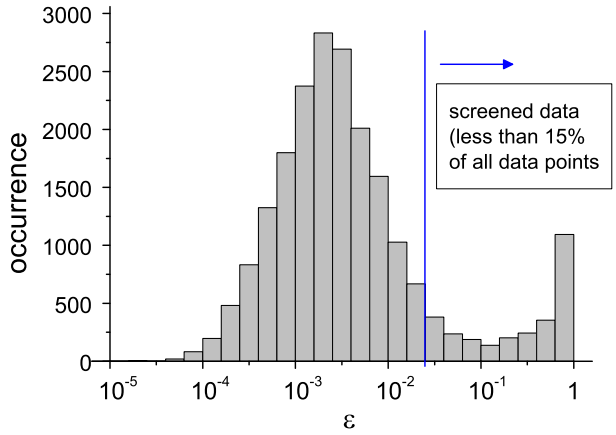

Fig. 2. Histogram for the values of ϵ as determined from all MFRSR PWV data of 2005–2009. We define the data with $\epsilon > 10^{-1.6}$ as not reliable.

AMTD
2, 1625–1662, 2009

Quality assessment of upper-air water vapour techniques

M. Schneider et al.

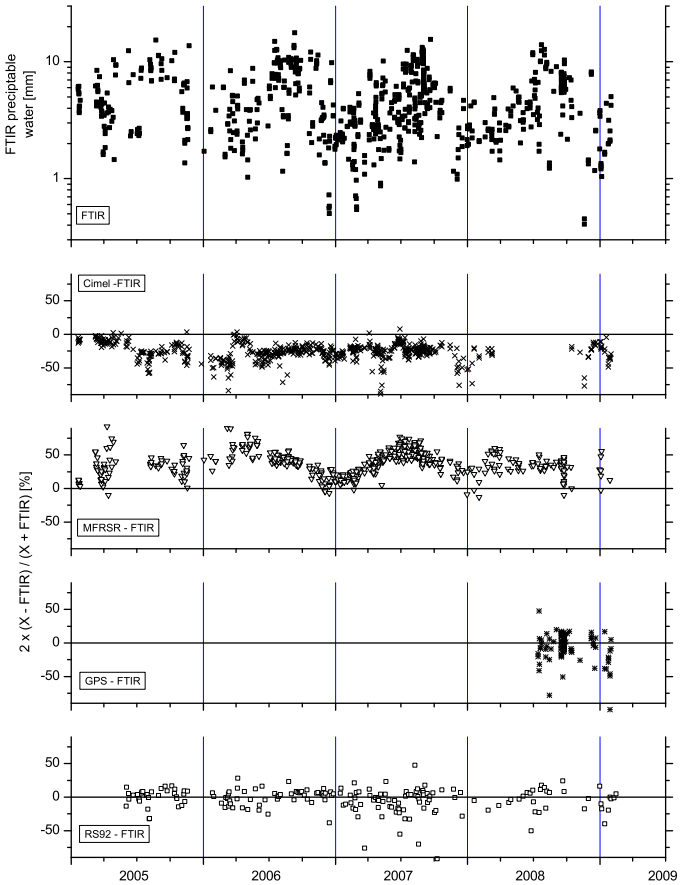

Fig. 3. Time series of Izaña's PWV measurements. Upper panel: PWV as measured by FTIR; Rest of the panels: Difference between FTIR and the other techniques $\left(\frac{2\times(X-FTIR)}{(X+FTIR)}\right)$, where X is Cimel, MFRSR, GPS, and RS92, as given in the panels, respectively.

AMTD
2, 1625–1662, 2009

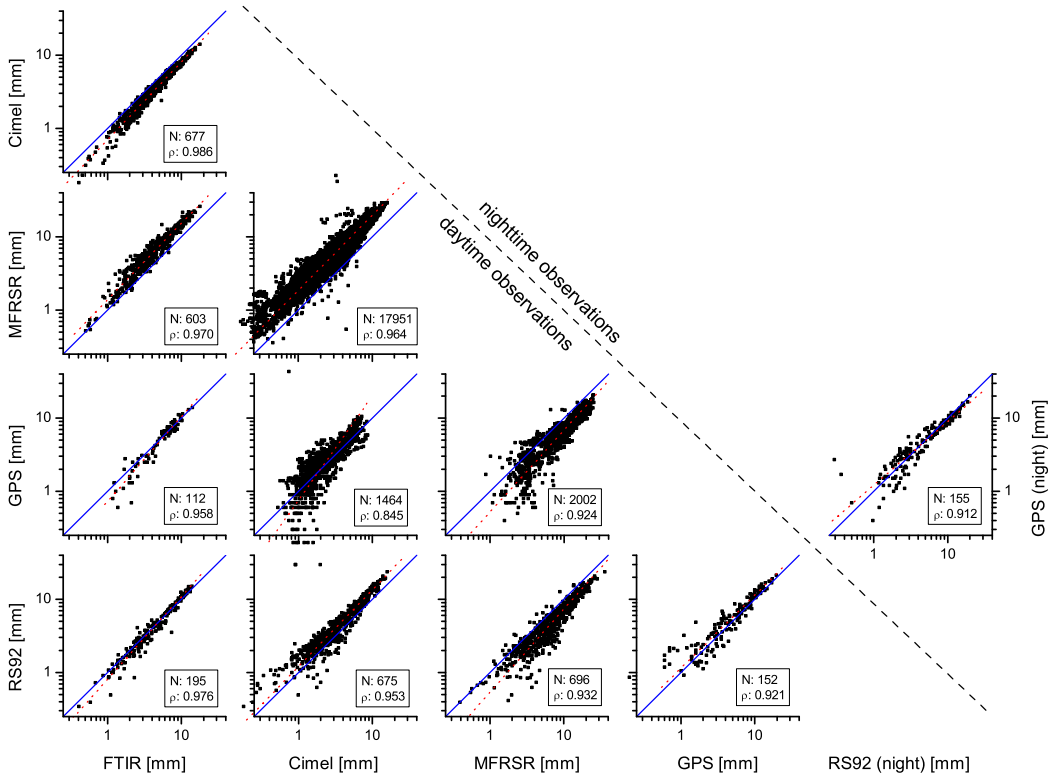

Fig. 4. Correlation of PWVs measured by FTIR, Cimel, MFRSR, GPS, and Vaisala RS92. The number of coincidences N and the correlation coefficients ρ are given in each panel. The blue line is the diagonal and the red dotted line the linear regression line.

AMTD
2, 1625–1662, 2009

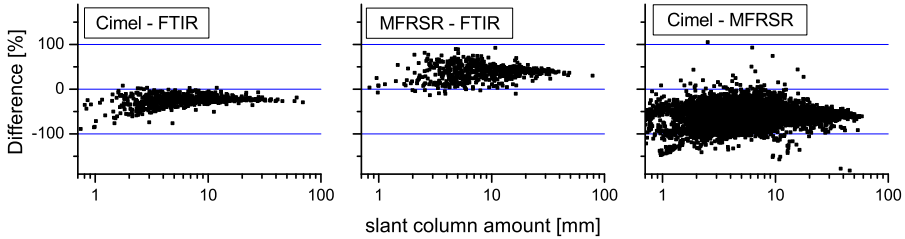

Fig. 5. Estimation of the dependence of the PWVs of FTIR, Cimel, and MFRSR on the observed water vapour slant column amount. Plotted are the differences of the PWVs versus the slant column amounts. Left panel: $2\times\frac{\text{Cimel}-\text{FTIR}}{\text{Cimel}+\text{FTIR}}$; Middle panel: $2\times\frac{\text{MFRSR}-\text{FTIR}}{\text{MFRSR}+\text{FTIR}}$ (top panels); Right panel: $2\times\frac{\text{Cimel}-\text{MFRSR}}{\text{Cimel}+\text{MFRSR}}$.

AMTD
2, 1625–1662, 2009

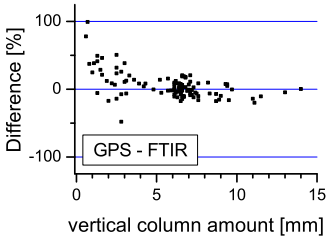

Fig. 6. Dependence of $2\times\frac{\text{GPS}-\text{FTIR}}{\text{GPS}+\text{FTIR}}$ on PWVs.

AMTD
2, 1625–1662, 2009

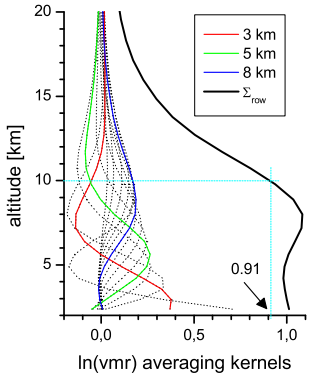

Fig. 7. Typical averaging kernels for ground-based FTIR remote sensing of water vapour. The kernels for 3, 5, and 8 km are highlighted by red, green, and blue colors, respectively. The total sensitivity ($\sum_{row}$) is depicted as thick black line.

AMTD
2, 1625–1662, 2009

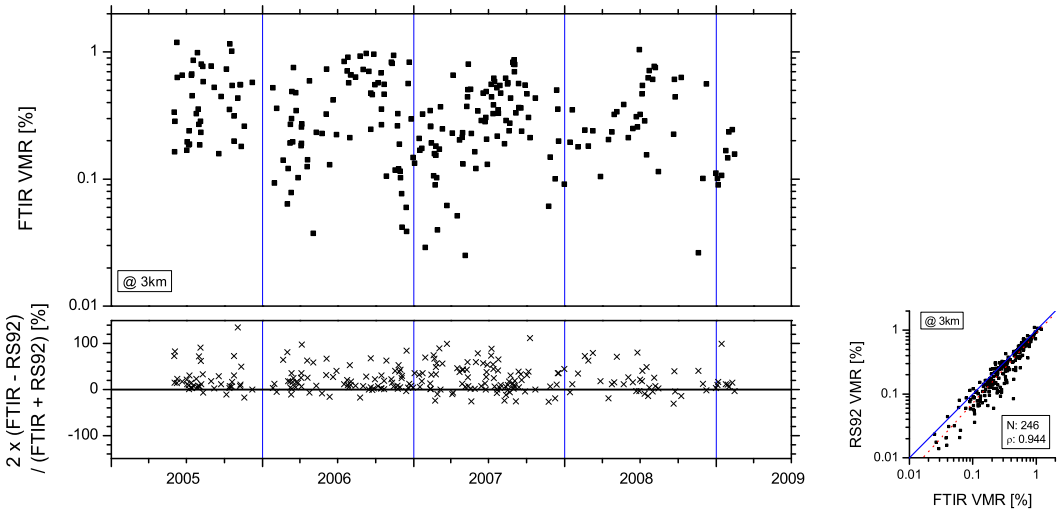

Fig. 8. Comparison of RS92 and FTIR lower tropospheric (altitude of 3 km) water vapour mixing ratios, whereby the RS92 mixing ratios have been smoothed according to Eq. (1). Left panels: time series for FTIR/RS92 coincidences, top panel: FTIR mixing ratios given in percent (1 water molecule per 100 air molecules), bottom panel: difference between FTIR and RS92 $\left(\frac{2\times(\mathrm{FTIR}-\mathrm{RS92})}{(\mathrm{FTIR}+\mathrm{RS92})}\right)$; Right panel: correlation plot for all coincident measurements between 2005 and 2009.

AMTD
2, 1625–1662, 2009

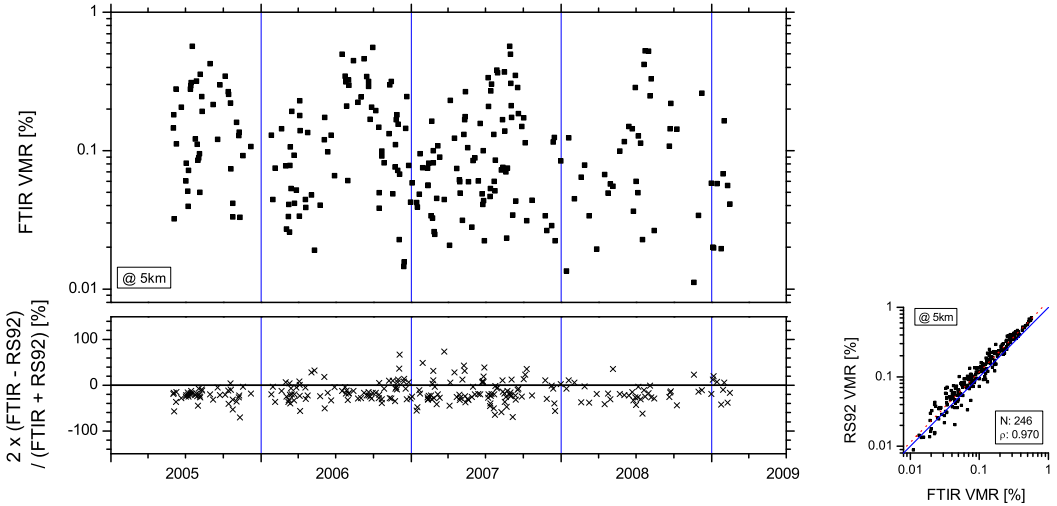

Fig. 9. Same as Fig. 8 but for the middle troposphere (altitude of 5 km).

AMTD
2, 1625–1662, 2009

Quality assessment of upper-air water vapour techniques

M. Schneider et al.

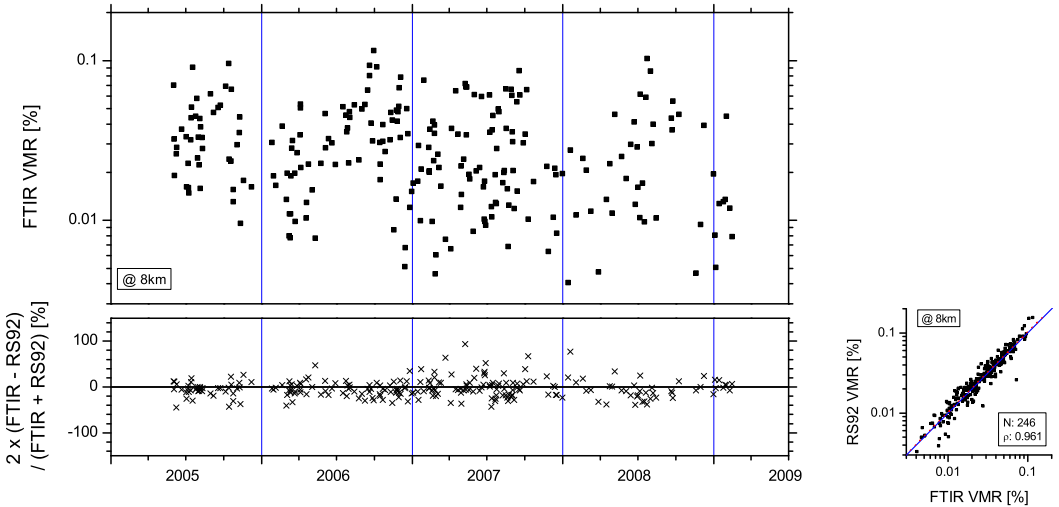

Fig. 10. Same as Fig. 8 but for the upper troposphere (altitude of 8 km).

AMTD
2, 1625–1662, 2009

Quality assessment of upper-air water vapour techniques

M. Schneider et al.

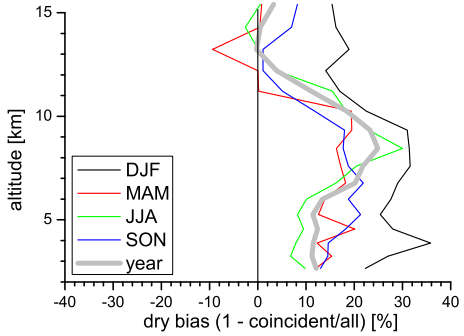

Fig. 11. Vertical profiles of the FTIR dry bias B, for winter (black line), spring (red line), summer (green line), autumn (blue line), and all season (thick grey line).

AMTD
2, 1625–1662, 2009